Universität Potsdam

Mathematisch-Naturwissenschaftliche Fakultät

Humaad Ghani | Edward R. Sobel | Gerold Zeilinger | Johannes Glodny | Sebastian Zapata | Irum Irum

Palaeozoic and Pliocene tectonic evolution of the Salt Range constrained by low-temperature thermochronology

Suggested citation referring to the original publication:
Terra nova 33 (2020) 3, pp. 293 - 305
DOI https://doi.org/10.1111/ter.12515
ISSN 0954-4879, 1365-3121

Journal article | Version of record

Secondary publication archived on the Publication Server of the University of Potsdam:
Zweitveröffentlichungen der Universität Potsdam : Mathematisch-Naturwissenschaftliche Reihe 1368
ISSN: 1866-8372
https://nbn-resolving.org/urn:nbn:de:kobv:517-opus4-562567
DOI: https://doi.org/10.25932/publishup-56256

Terms of use:
This work is licensed under a Creative Commons License. This does not apply to quoted content from other authors. To view a copy of this license visit https://creativecommons.org/licenses/by/4.0/.

Received: 22 October 2020 | Revised: 10 November 2020 | Accepted: 22 November 2020

DOI: 10.1111/ter.12515

RESEARCH ARTICLE

Terra Nova WILEY

Palaeozoic and Pliocene tectonic evolution of the Salt Range constrained by low-temperature thermochronology

Humaad Ghani[1] | Edward R. Sobel[1] | Gerold Zeilinger[1] | Johannes Glodny[2] | Sebastian Zapata[1,3,4] | Irum Irum[1]

[1]Institute of Geosciences, University of Potsdam, Potsdam, Germany

[2]GFZ German Research Center for Geosciences, Potsdam, Germany

[3]Smithsonian Tropical Research Institute, Balboa, Ancon, Panama

[4]Department of Geosciences and Geological and Petroleum Engineering, Missouri University of Science and Technology, USA

Correspondence
Humaad Ghani, Institute of Geosciences, University of Potsdam, Potsdam, Germany.
Email: hammadtanoli@gmail.com

Funding information
German Academic Exchange Service (DAAD); DFG

Abstract

The Salt Range in Pakistan exposes Precambrian to Pleistocene strata outcropping along the Salt Range Thrust (SRT). To better understand the in-situ Cambrian and Pliocene tectonic evolution of the Pakistan Subhimalaya, we have conducted low-temperature thermochronological analysis using apatite (U-Th-Sm)/He and fission track dating. We combine cooling ages from different samples located along the thrust front of the SRT into a thermal model that shows two major cooling events associated with rifting and regional erosion in the Late Palaeozoic and SRT activity since the Pliocene. Our results suggest that the SRT maintained a long-term average shortening rate of ~5–6 mm/yr and a high exhumation rate above the SRT ramp since ~4 Ma.

KEYWORDS

exhumation, fault bend fold, ramp, Salt Range

1 | INTRODUCTION

Low-temperature thermochronological data coupled to structural data can provide constraints on the structural evolution and long-term exhumation history of relatively shallow (2–5 km deep) crustal levels. Therefore, previous thermochronological and magnetostratigraphic studies of the Subhimalaya have used Neogene foreland strata to examine the Cenozoic deformational history (e.g. Burbank et al., 1996; Gavillot et al., 2018; van der Beek et al., 2006). However, limited or non-existent exposure of Palaeozoic–Mesozoic bedrock strata in the Indian and Nepalese Subhimalaya has precluded robust constraints on the regional pre-collisional history and possible influence of structural inheritance on the Cenozoic history. The Palaeozoic to Mesozoic strata exposed in the Salt Range (SR; Figure 1) has the potential to record pre-Cenozoic thermal and cooling events from low-temperature thermochronometers because of limited (~2–5 km) burial beneath Cenozoic foreland sediment.

We present here the first low-temperature thermochronological dataset from samples collected along the strike of the SR. Structural, stratigraphic and bedrock detrital cooling data from each sample were combined within a single thermal model to extract quantitative thermal history constraints. The thermal model and structural reconstructions are used to document the Palaeozoic deformational event and long-term thermotectonic evolution of the Salt Range thrust (SRT).

2 | TECTONIC FRAMEWORK AND STRATIGRAPHY

The Pakistan Subhimalaya is defined by the Kohat and Potwar (Figure 1). These are bounded to the north by the Main Boundary

This is an open access article under the terms of the Creative Commons Attribution License, which permits use, distribution and reproduction in any medium, provided the original work is properly cited.
© 2020 The Authors. Terra Nova published by John Wiley & Sons Ltd.

Thrust (MBT), which formed at around ~10 Ma (Brozovic & Burbank, 2000; Meigs et al., 1995; Turab et al., 2017). At the southern border of the Potwar, the SRT lifts up Precambrian to Pliocene strata above the SRT ramp and exposes them in a fault bend fold above Quaternary sediments of the Punjab Plain (Figure 1; Baker et al., 1988; Ghani et al., 2018). The stratigraphy in the SR is subdivided into three major units: (a) Late Neoproterozoic to Lower Cambrian evaporites, (b) Cambrian to Eocene siliciclastic and carbonate sequences, and (c) Miocene to Pliocene foreland strata derived from erosion of the Himalayan orogen (Gee & Gee, 1989; Figure 2, Supplementary material section 1).

Statement of Significance

This study presents the first thermochronological dataset from the Palaeozoic rocks of the Subhimalaya. In order to understand the in-situ basin thermal history, we have adopted a new thermal modelling approach based on joint modelling of different stratigraphic age samples collected from multiple, structurally similar transects in the Salt Range. The thermal models show that the Salt Range area experienced a major exhumation event in the Late Palaeozoic before Cenozoic formation of the Salt Range, part of the Himalayan range front. The results of this study provide new constraints on rates of shortening and exhumation for the Salt Range Thrust.

3 | THERMOCHRONOLOGICAL RESULTS, ANALYSIS AND THERMAL HISTORY CONSTRAINTS

Samples were collected from Cambrian, Permian, Mesozoic and Miocene strata exposed in four transects along the hanging wall of the SRT (Figures 1 and 2). The Khewra, Karoli and Pail transects are located along the thrust front of the SRT; the Western SR is located along the lateral ramp of the SRT. Apatite (U-Th-Sm)/He (AHe) dating was performed on 16 samples. A total of 61 single-grain AHe cooling ages are dispersed between 0.8 and 136 Ma; the majority are <10 Ma (Figure 2). Fifteen samples were used for apatite fission track (AFT) dating; 11 yielded confined track lengths (TL; Tables 1 and 2). Mean TL range from 9 to 12.8μm. The AFT central ages of Cambrian and Permian samples from the Khewra, Karoli and Pail transects span from 205 ± 9 to 249 ± 13 Ma, except for a granite clast (sample TgKr) that has the oldest age of 355 ± 15 Ma. In the Western SR, AFT central ages of Permian samples span from 3.7 ± 0.7 to 238 ± 15 Ma. The two Miocene age samples KmPa and KmKr are located ~15 km north of the thrust front. Six single-grain AHe ages from these samples are around ~2 Ma; a single grain is ~7 Ma. Only sample KmPa was used for AFT analysis, yielding a central age of 28 ± 2 Ma. The AHe and AFT methods are sensitive to temperatures of ~40–80°C (the apatite helium partial retention zone, AHePRZ) and 60–120°C (the apatite partial annealing zone, APAZ) respectively (Farley, 2000, 2002; Gallagher et al., 1998). Details about dating methods, AFT age population analysis and the calculation of AFT central ages are provided in supplementary material section 2.

The Palaeozoic–Cenozoic stratigraphic wedge thickness above the Salt Range Formation increases northward from ~2.5 km along the SRT range front to ~5 km, where the northernmost sample TbDk was collected (Figure 2). The large AFT age dispersion (~4–355 Ma) is related to the estimated thickness of the stratigraphic overburden at each sample location prior to Late-Cenozoic exhumation (Figure 2; Table 3). Approximately 3 km of Cenozoic strata exposed above the SRT ramp suggest that the Cambrian and Permian samples in the Khewra, Karoli and Pail transects along the thrust front were subjected to roughly equal stratigraphic burial before exhumation. Assuming a ~20°C surface temperature and a geothermal gradient of ~25°C/km (Gavillot et al., 2018; Kadri, 1995; Khan & Raza, 1986), the estimated Cenozoic burial temperature for these samples ranges between 70 and 95°C, implying that AFT ages are partially reset and AHe ages are partially to fully reset (Figure 2). The samples in the Western SR have northward-younging AFT ages and decreasing TL from the Ghundi lobe (Figures 1 and 2), implying significant post-depositional heating and subsequent exhumation. The northernmost sample TbDk is estimated to have been buried ~5 km beneath Mesozoic and Cenozoic sediment prior to exhumation; this depth implies palaeotemperatures of 120–145°C, sufficient to fully reset AFT and AHe ages. The Miocene samples were estimated to have been buried to ~3 km beneath foreland strata, implying a palaeotemperature of ~95°C, sufficient to fully reset AHe ages but not AFT ages.

4 | THERMAL MODELLING APPROACH AND RESULTS

We used the QTQt program (Gallagher, 2012) for inverse modelling of low-temperature thermochronological data to find possible time-temperature histories of the samples. Four parameters from each sample (if available) were used: AFT central (population) age, C-axis projected TL, Dpar and single-grain AHe ages (Table 4). Cambrian, Permian, Palaeogene and Miocene stratigraphic succession were used as geological constraints in the Khewra, Karoli and Pail transects, assuming that samples were close (0–30°C) to the surface temperatures during these periods of sedimentation.

FIGURE 1 (a) Structural map of the Salt Range and its surrounding regions (modified after Gee & Gee, 1989; Ghani et al., 2018). The inset shows Pakistan and its neighbouring countries. (b) Generalised stratigraphy of the Salt Range and stratigraphic location of the samples. (c) Geographic location of the samples [Colour figure can be viewed at wileyonlinelibrary.com]

13653121, 2021, 3, Downloaded from https://onlinelibrary.wiley.com/doi/10.1111/ter.12515 by Universitaetsbibliothek, Wiley Online Library on [22/09/2023]. See the Terms and Conditions (https://onlinelibrary.wiley.com/terms-and-conditions) on Wiley Online Library for rules of use; OA articles are governed by the applicable Creative Commons License

(a)

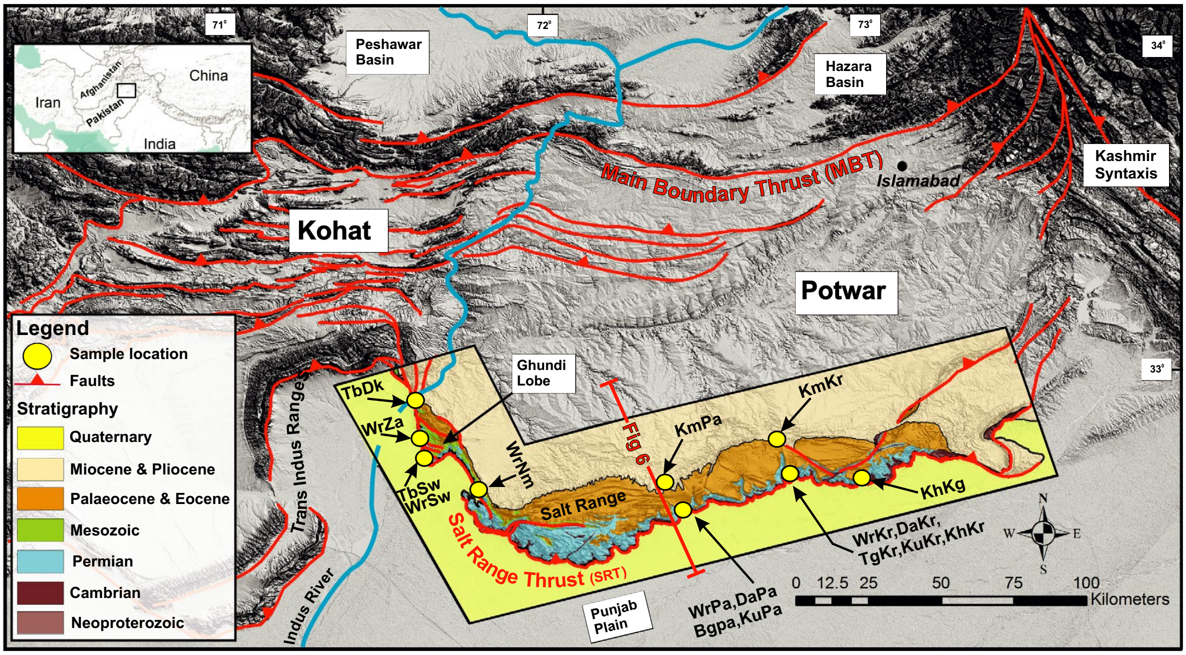

(b)

AGE			Formations
ERA	PERIOD	EPOCH	
CENOZOIC	QUATERNARY	PLEISTOCENE	Kalabagh Conglomerate
		~2.5 Ma	
	TERTIARY	PLIOCENE	Siwalik Group: Soan; DHOK PATHAN; Nagri; Chingi
		~5 Ma	
		MIOCENE	Rawalpindi Group: Kamlial; Murree
		~23 Ma	
		OLIGOCENE	Unconformity
		~34 Ma	
		EOCENE	Chorgali, Sakesar, Nammal
		~56 Ma	
		PALAEOCENE	Patala, Lockart, Hangu
		~66 Ma	Unconformity
MESOZOIC	CRETACEOUS		Lamshiwal, Chichali
		~145 Ma	
	JURASSIC		Samanasuk, Shinawri, Datta
		~200 Ma	
	TRIASSIC		Kingriali, Tridian, Mianwali
			Unconformity
		~250 Ma	
PALAEOZOIC	PERMIAN		Chiddru, Wargal, Amb, Sardai, Warcha, Dandot, Tobra
		~300 Ma	
	CARBONIFEROUS – ORDOVICIAN		Unconformity
		~485 Ma	
	CAMBRIAN		Baghanwala, Juttana, Kussak, Khewra
		~540 Ma	
NEOPROTEROZOIC			Salt Range Formation

(c)

Sample	Formation	Elevation (m)	Latitude (N)	Longitude (E)	AHe data	AFT data
KhKg	Khewra	390	32.6688°	73.0051°	X	X
KhKr	Khewra	540	32.6747°	72.7783°	X	X
KuKr	Kussak	610	32.6766°	72.7766°	X	X
TgKr	Tobra	620	32.6769°	72.7766°	X	X
DaKr	Dandot	625	32.6770°	72.7766°	X	–
WrKr	Warcha	700	32.6808°	72.7736°	X	X
KmKr	Kamlial	710	32.7681°	72.7261°	X	–
KuPa	Kussak	355	32.5612°	72.4642°	X	X
BgPa	Baghanwala	440	32.5578°	72.4518°	X	X
DaPa	Dandot	460	32.5586°	72.4514°	–	X
WrPa	Warcha	490	32.5640°	72.4542°	X	X
KmPa	Kamlial	720	32.6718°	72.3726°	X	X
WrNm	Warcha	480	32.5972°	71.8167°	X	X
WrSw	Warcha	295	32.7042°	71.6431°	X	X
TbSw	Tobra	280	32.7258°	71.6322°	X	X
WrZa	Warcha	310	32.7808°	71.5406°	X	X
TbDk	Tobra	260	32.9097°	71.6042°	X	X

13653121, 2021, 3, Downloaded from https://onlinelibrary.wiley.com/doi/10.1111/ter.12515 by Universitaetsbibliothek, Wiley Online Library on [22/09/2023]. See the Terms and Conditions (https://onlinelibrary.wiley.com/terms-and-conditions) on Wiley Online Library for rules of use; OA articles are governed by the applicable Creative Commons License

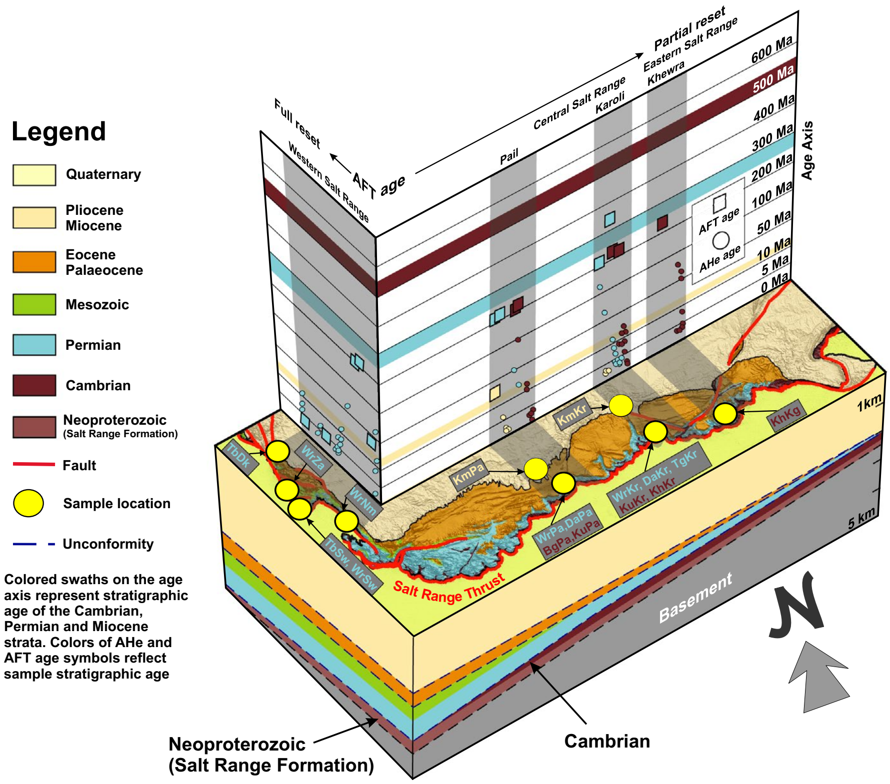

FIGURE 2 (a) Geological block diagram showing the geometry of the stratigraphic wedge, surficial geology, sample locations and their respective AHe and AFT ages in the Salt Range. Thicknesses of different stratigraphic units in the block diagram beneath the map are estimated from map relationships and cross-sections (Gee & Gee, 1989; Ghani et al., 2018). Note that the scale on the age axis is not linear; but selected to better show the spatial distribution of AFT and AHe ages [Colour figure can be viewed at wileyonlinelibrary.com]

We used three different modelling approaches (M1, M2, M3). In M1, we model data from individual samples from different transects, assuming that samples have experienced different burial depths, and therefore do not share a similar thermal history (Figure 3). Because KhKg and the Karoli and Pail transects have similar palaeotemperature constraints, we modelled KhKg using M1 to compare the M1 and M2 results. In M2, we combined data from Cambrian and Permian depositional-age samples from the same stratigraphic transect into a single thermal model for the Karoli and Pail transects and from two Western SR Permian samples (TbSw and WrSw; Figure 3). Our second approach is based on the assumption that, although the samples have different stratigraphic ages, they experienced a similar post-depositional thermal history.

In M3, we combined all Cambrian and Permian depositional-age sample data from the Khewra, Karoli and Pail transects into one single pseudo-stratigraphic transect for thermal modelling (Figure 4). The sampled locations can be combined because they share similar structural positions along the strike of the SRT and stratigraphic overburden (~3 km) beneath foreland strata, and as shown by the models obtained in the first two approaches, experienced similar thermal histories (Figures 2 and 3). Samples from the Western SR were not included in this joint model because they are located on the lateral ramp of the SRT and were buried to different depths (Figure 2). Similarly, samples KmPa and KmKr were not included in the model because they are located ~20 km north of modelled samples on the SRT ramp and have experienced different burial depths.

The thermal model results for M3 (Figure 4) suggest that Cambrian samples were heated up to ~75 to ~100°C between ~500 and ~370 Ma, partially resetting the AFT ages. Cooling commenced in Late Devonian time and persisted to Permian time. The samples remained colder than ~70°C from Permian to Miocene time. The final heating, up to ~80 to ~105°C, occurred in the Middle to Late Miocene, totally resetting the majority of the AHe ages, partially resetting all AFT ages, and moderately annealing track lengths. Final rapid cooling occurred from ~4 to ~3 Ma; afterwards, samples cooled very slowly to surface temperature.

Modelling results in Figure 4 show the single paths (maximum likelihood) for each sample that best fit the observed data and the average paths (expected) of all acceptable paths of the thermal model. The maximum likelihood path is ~10°C hotter in Middle-to-Late Devonian time than the expected path and stays up to ~30°C colder from the Permian to the Miocene. The maximum likelihood path fits almost all AFT and TL data compared to the poorer fit of the expected model; however, both models only fit young (<5 Ma) AHe ages (Figure 4b).

5 | THERMAL MODEL GEOLOGICAL INTERPRETATION AND DISCUSSION

5.1 | Cambrian to Permian basin history

Shallow-marine Cambrian clastic sediments were deposited on top of Late Neo-Proterozoic-Lower Cambrian Salt (Hughes et al., 2019, and references therein). The thermal models of all Cambrian samples suggest that the AFT system in SR Cambrian strata must have been heated and partially reset during the early Palaeozoic (Figures 3

13653121, 2021, 3, Downloaded from https://onlinelibrary.wiley.com/doi/10.1111/ter.12515 by Universitaetsbibliothek, Wiley Online Library on [22/09/2023]. See the Terms and Conditions (https://onlinelibrary.wiley.com/terms-and-conditions) on Wiley Online Library for rules of use; OA articles are governed by the applicable Creative Commons License

TABLE 1 Apatite (U-Th-Sm/He) data of samples from the Salt Range, Pakistan

Sample	F_T corrected Age (Ma)	Weighted 2σ analytic error (Ma)	U (ppm)	Th (ppm)	^{147}Sm (ppm)	e[U] (ppm)	Th/U	He (nmol/g)	mass (µg)	F_T	ESR (µm)	uncorrected Age (Ma)	unweighted 2σ analytic error (Ma)
Khewra Transect													
KhKg_1	2.6	0.3	15.9	28.2	18.7	22.6	1.83	0.22	1.99	0.68	46	1.8	0.2
KhKg_2	5.5	0.6	18.5	39.3	60.7	27.8	2.19	0.47	0.86	0.56	34	3.2	0.4
KhKg_3*	47.3	4.3	0.8	4.6	14.3	1.9	5.84	0.33	1.58	0.64	42	31.0	3.1
KhKg_4	2.6	0.6	6.5	37.3	25.7	15.3	5.94	0.13	1.19	0.61	38	7.8	0.3
KhKg_5	81.4	1.6	38.4	125.1	70.1	67.8	3.37	18.70	1.45	0.62	39	50.4	2.0
Karoli Transect													
KhKr_1	19.4	0.4	71.7	38.6	21.1	80.8	0.56	6.13	3.31	0.72	54	14.0	0.5
KhKr_2	10.1	0.5	24.1	28.7	54.6	30.8	1.23	1.03	1.22	0.61	38	6.1	0.4
KhKr_3	3.4	0.8	3.6	24.3	18.0	9.3	7.06	0.11	1.58	0.64	42	2.1	0.5
KhKr_4	6.7	0.2	48.4	133.5	100.6	79.8	2.85	2.12	3.85	0.73	55	4.8	0.1
KhKr_5*	34.9	0.8	25.5	64.2	39.2	40.5	2.60	5.51	2.93	0.71	52	24.9	1.2
KuKr_1	1.9	0.3	9.0	89.5	48.6	30.0	10.31	0.19	1.03	0.59	37	1.1	0.1
KuKr_2*	20.3	1.1	13.0	109.5	73.7	38.7	8.71	2.37	0.74	0.55	33	11.0	0.7
KuKr_3	10.0	1.0	7.4	47.9	21.3	18.7	6.67	0.60	1.02	0.59	36	5.8	0.6
KuKr_4	10.2	0.3	48.1	108.3	12.8	73.6	2.33	2.33	0.95	0.57	35	5.8	0.2
TgKr_1	17.7	0.7	8.8	35.3	28.3	17.1	4.14	1.06	1.55	0.64	41	11.2	0.5
TgKr_2	4.9	0.8	6.9	35.4	37.2	15.2	5.31	0.24	0.96	0.57	35	2.9	0.5
TgKr_3	3.8	0.3	10.3	37.8	29.3	19.2	3.79	0.26	1.86	0.65	43	2.4	0.2
TgKr_4	9.3	0.3	4.2	15.9	18.3	7.9	3.95	0.30	4.23	0.74	58	6.9	0.2
TgKr_5	7.7	0.4	6.6	34.4	28.7	14.7	5.37	0.43	2.78	0.69	49	5.3	0.3
DaKr_1	5.5	0.4	11.6	18.6	9.4	15.9	1.66	0.33	2.49	0.69	48	3.8	0.3
DaKr_2	4.0	0.1	33.1	52.6	26.7	45.4	1.65	0.75	6.88	0.77	65	3.0	0.1
DaKr_3	2.9	0.5	1.7	5.4	12.1	3.0	3.27	0.04	5.51	0.76	62	2.1	0.3
DaKr_4	3.8	0.2	13.2	21.8	37.4	18.3	1.70	0.28	5.10	0.75	59	2.8	0.1
WrKr_1*	70.4	1.5	20.9	44.1	34.0	31.2	2.18	8.15	2.50	0.68	47	47.7	1.6
WrKr_2*	135.9	6.9	3.4	8.8	28.2	5.5	2.63	2.67	1.40	0.63	41	85.7	7.7
KmKr_1	2.4	0.1	9.7	49.8	11.6	21.5	5.28	0.22	6.10	0.77	65	1.8	0.1
KmKr_2	1.4	0.1	23.0	105.0	10.1	47.6	4.72	0.28	6.48	0.78	68	1.0	0.1
KmKr_3	2.2	0.1	13.4	63.8	18.8	28.4	4.93	0.28	12.71	0.82	83	1.8	0.1
Pail Transect													
BgPa_1*	0.8	0.1	121.6	156.8	78.2	158.4	1.33	0.41	1.39	0.62	40	0.4	0.1
BgPa_2	4.1	0.1	10.7	121.9	43.9	39.3	11.78	0.60	2.08	0.68	46	2.7	0.1
BgPa_3	29.0	2.1	2.5	30.4	24.5	9.6	12.58	0.88	0.83	0.56	34	16.8	1.7

(Continues)

13653121, 2021, 3, Downloaded from https://onlinelibrary.wiley.com/doi/10.1111/ter.12515 by Universitaetsbibliothek, Wiley Online Library on [22/09/2023]. See the Terms and Conditions (https://onlinelibrary.wiley.com/terms-and-conditions) on Wiley Online Library for rules of use; OA articles are governed by the applicable Creative Commons License

TABLE 1 (Continued)

Sample	F_T corrected Age (Ma)	Weighted 2σ analytic error (Ma)	U (ppm)	Th (ppm)	^{147}Sm (ppm)	e[U] (ppm)	Th/U	He (nmol/g)	mass (µg)	F_T	ESR (µm)	uncorrected Age (Ma)	unweighted 2σ analytic error (Ma)
BgPa_4	4.5	0.7	2.0	32.7	18.7	9.7	16.57	0.14	0.98	0.58	36	2.7	0.5
KuPa_1	3.1	0.6	5.4	8.8	17.6	7.4	1.68	0.09	2.26	0.69	48	2.0	0.3
KuPa_2*	113.7	1.3	25.1	38.2	19.0	34.1	1.57	14.33	2.30	0.68	47	77.0	1.7
KuPa_3	3.4	0.7	11.3	34.0	17.9	19.3	3.12	0.21	0.98	0.58	36	1.9	0.3
KuPa–4	17.1	2.2	8.5	9.8	10.3	10.8	1.20	0.57	0.89	0.57	35	9.7	1.4
WrPa–2	32.2	1.1	8.2	29.8	87.0	15.2	3.76	2.05	4.37	0.74	58	23.8	1.5
WrPa–3*	51.7	2.7	5.5	29.7	27.3	12.4	5.63	2.17	1.26	0.61	39	31.6	2.3
KmPa_1	2.3	0.3	4.0	12.5	20.4	6.9	3.24	0.07	5.98	0.76	63	1.7	0.2
KmPa_2	7.0	0.3	9.6	48.6	30.2	21.0	5.23	0.60	5.01	0.74	58	5.2	0.2
KmPa_3	2.0	0.2	4.1	11.5	10.4	6.8	2.92	0.06	7.95	0.79	71	1.5	0.1
KmPa_4	1.6	0.1	4.7	26.3	8.5	10.8	5.82	0.08	7.89	0.79	72	1.2	0.1
Western Salt Range Transect													
WrNm_1	2.6	0.2	1.1	21.2	18.3	6.1	19.94	0.07	14.52	0.83	89	2.1	0.2
WrNm_2*	68.3	3.0	0.7	24.0	17.3	6.3	37.32	1.48	1.29	0.62	39	42.0	5.9
WrNm_3	9.9	0.8	3.9	19.1	8.3	8.4	5.10	0.33	3.10	0.72	54	7.0	0.6
WrNm_4	24.0	1.1	3.3	16.1	33.8	7.0	5.10	0.79	16.35	0.84	92	20.0	1.6
WrSw_1	9.6	0.6	3.5	82.8	27.1	22.9	24.67	0.92	5.54	0.77	65	7.3	0.8
WrSw_2	17.5	0.6	58.7	39.3	40.1	67.9	0.69	3.66	1.01	0.57	35	9.9	0.5
WrSw_3	5.1	1.2	12.4	23.5	18.9	17.9	1.97	0.27	0.83	0.55	33	2.9	0.7
WrSw_4	8.0	0.5	8.4	17.8	8.9	12.6	2.19	0.41	4.48	0.75	61	6.0	0.8
TbSw_1	10.1	1.3	14.8	56.1	11.4	28.0	3.92	0.85	0.80	0.56	34	5.7	1.2
TbSw_2	6.4	1.1	8.1	32.8	21.4	15.8	4.19	0.34	1.24	0.62	39	4.0	0.2
TbSw_3	4.3	1.0	3.5	1.6	11.0	3.9	0.48	0.07	3.75	0.73	56	3.1	0.8
TbSw_4	4.3	0.6	4.7	54.2	13.8	17.4	11.89	0.26	1.62	0.64	42	2.8	0.4
TbSw_5*	70.1	2.8	19.9	29.3	28.4	26.8	1.52	7.32	2.95	0.71	52	50.1	4.4
WrZa_1	3.0	0.3	5.0	16.9	34.0	8.9	3.5	0.1	7.92	0.79	72	2.4	0.3
WrZa_2	1.7	0.3	2.4	51.9	20.3	14.6	22.63	0.10	3.70	0.74	57	1.3	0.2
WrZA_3	7.0	0.3	7.8	48.1	28.9	19.1	6.4	0.6	24.91	0.86	107	6.0	0.4
TbDk_1	8.8	1.3	6.5	16.0	16.0	10.3	2.55	0.31	1.36	0.63	41	5.7	1.1
TbDk_2	5.2	0.5	6.5	17.8	14.5	10.7	2.84	0.22	4.21	0.74	58	3.8	0.3
TbDk_4*	17.0	0.4	17.0	5.4	19.1	18.3	0.33	1.40	13.54	0.82	85	14.0	0.6

Note: Ages are reported as single-grain cooling ages. Ages marked with (*) are not used in the thermal models because the age did not fit the intra-sample eU versus age trend, or the grain has an older ages but a similar eU value compared to other grains from the same sample.

Abbreviations: F_T, Correction factor for He ejection/diffusion; e[U], Effective uranium content; ESR, Equivalent spherical radius.

13653121, 2021, 3, Downloaded from https://onlinelibrary.wiley.com/doi/10.1111/ter.12515 by Universitaetsbibliothek, Wiley Online Library on [22/09/2023]. See the Terms and Conditions (https://onlinelibrary.wiley.com/terms-and-conditions) on Wiley Online Library for rules of use; OA articles are governed by the applicable Creative Commons License

TABLE 2 Apatite fission track data of samples from the Salt Range, Pakistan

Sample	N	N_s	ρ_s	N_i	ρ_i	N_d	ρ_d	$P_{(\chi 2)\%}$	Sample Age ± 1σ	Populations Age ± 1σ (n)	$P_{(\chi 2)\%}$	(nTL)	MTL ± 1σ (μm)	TLSD (μm)	Dpar (μm)	Dpar SD (μm)
KhKg	23	1,287	17.1	1839	24.5	8,035	13.0	0	162 ± 20	249 ± 13 (14)*	98	61	9.78	1.51	2.14	0.24
										131 ± 10 (5)	69					
KhKr	22	1,425	12.0	1611	13.6	8,035	13.0	0.6	196 ± 12	216 ± 10 (17)*	98	41	9.11	1.57	2.21	0.33
										112 ± 13 (5)	90					
KuKr	20	936	14.3	1,257	19.2	8,035	13.3	0.03	174 ± 13	220 ± 13 (11)*	99					
										122 ± 9 (9)	99					
TgKr	22	2021	11.6	1,230	7.4	8,035	13.1	96	355 ± 15*			100	10.59	1.35	2.06	0.21
WrKr	20	1884	15.7	2,225	18.6	8,035	13.1	0.09	196 ± 10	203 ± 9 (19)*	42	34	11.02	1.51	2.12	0.26
KuPa	20	1,443	17.3	2,499	30.0	8,035	13.1	0	155 ± 18	205 ± 10 (14)*	90					
BgPa	20	1,033	13.4	1,660	21.5	8,035	13.0	0	141 ± 21	230 ± 13 (12)*	99	37	9.92	1.31	2.25	0.35
										40 ± 4 (6)	83					
DaPa	20	1,210	15.9	1,327	17.4	8,035	13.0	0	200 ± 16	229 ± 11 (17)*	99	41	9.51	1.42	1.96	0.24
WrPa	20	1,720	14.7	2,115	18.1	8,035	13.1	0.02	189 ± 11	205 ± 9 (18)*	98	24	10.32	1.12	2.33	0.36
KmPa	18	453	2.8	4,726	29.1	8,035	13.1	0	21 ± 2	28 ± 2 (13)*	70	13	12.81	1.51	2.63	0.29
										12 ± 5 (5)	98					
WrNm	25	541	3.8	2,384	16.9	7,720	12.6	0	53 ± 6	44 ± 3 (20)*	99	9	9.13	1.53	2.24	0.22
TbSw	22	903	12.7	1,231	17.3	7,720	12.6	0	163 ± 25	238 ± 15 (13)*	43	44	9.81	1.92	2.54	0.54
										63 ± 6 (6)	47					
WrSw	20	850	9.6	886	10.0	7,720	12.6	32	209 ± 12	215 ± 8 (19)*	79	43	10.62	1.42	2.57	0.45
WrZa	22	298	2.3	2,876	22.4	7,720	12.5	0	27 ± 7	6 ± 1 (15)*	99					
TbDK	21	29	0.3	1758	19.4	7,720	12.6	69	3.7 ± 0.7*							

Note:: AFT ages are calculated by H. Ghani with Zeta (ζ) value = 353 ± 7. All AFT ages (sample and populations) are reported as central ages. The ages are divided into populations passing the χ^2 test. Track lengths are not necessarily measured in the same grain use for AFT age. The central ages marked with (*) are used for the thermal modelling in this study.

Notations: *N*: Number of grains; N_s: Number of spontaneous tracks measured in all apatite grains. N_i: Number of induced tracks measured in mica. ρ_s: Spontaneous track density, given as 10^5 tracks per cm^2. ρi: Induced track density, given as 10^5 tracks per cm^2. N_d: Number of tracks counted in dosimetry glass CN5. ρ_d: Dosimetry track density, given as 10^5 tracks per cm^2. $P_{(\chi 2)\%}$: Probability percentage of Chi-square (χ^2) value. nTL: Number of confined track lengths measured in a sample. MTL: Mean Track Length. Note that tracks lengths are projected parallel to the crystallographic c-axis for thermal modelling. TLSD: Standard deviation on the track length measurements. Dpar: Diameter of etch pits parallel to crystallographic c-axis of the crystal. Dpar *SD*: Standard deviation of the Dpar measurements.

13653121, 2021, 3, Downloaded from https://onlinelibrary.wiley.com/doi/10.1111/ter.12515 by Universitaetsbibliothek, Wiley Online Library on [22/09/2023]. See the Terms and Conditions (https://onlinelibrary.wiley.com/terms-and-conditions) on Wiley Online Library for rules of use; OA articles are governed by the applicable Creative Commons License

TABLE 3 Stratigraphic overburden and palaeotemperature estimates of samples from the Salt Range, Pakistan

Sample	Stratigraphic age (Ma)	Minimum stratigraphic overburden (m)	Temperature Range (min–max)
KhKg	500–550	2,500–3,000	82–95
KhKr	500–550	2,500–3,000	82–95
KuKr	500–550	2,500–3,000	82–95
TgKr	300–250	2,500–3,000	82–95
DaKr	300–250	2,500–3,000	82–95
WrKr	300–250	2,500–3,000	82–95
KmKr	16–18	2,500–3,000	82–95
KuPa	500–550	2,500–3,000	82–95
BgPa	500–550	2,500–3,000	82–95
DaPa	300–250	2,500–3,000	82–95
WrPa	300–250	2,500–3,000	82–95
KmPa	16–18	2,500–3,000	82–95
TbSw	300–250	2,500–3,000	82–95
WrSw	300–250	2,500–3,000	82–95
WrNm	300–250	3,000–3,500	95–108
WrZa	300–250	3,500–4,000	108–120
TbDk	300–250	4,000–5,000	120–145

Note.: Stratigraphic thickness is estimated from the structural cross section in Figure 6 and published studies (Gee & Gee, 1989; Ghani et al., 2018; Qayyum et al., 2015). Palaeotemperature range is estimated using ~ 20 ^{O}C surface temperature and the geothermal gradient ~25^{O}C/km.

and 4), most likely due to stratigraphic burial. About 2 km of Late Cambrian to Devonian strata are exposed in the adjacent Peshawar and Hazara Basins (Hughes et al., 2019; Pogue et al., 1992b). Therefore, we suggest that Ordovician to Devonian strata were present in the SR and buried the Cambrian strata before exhumation (Figure 5). The unconformity between Cambrian and Permian strata in the SR (Figures 1 and 2) was previously considered to be a depositional hiatus (Gee & Gee, 1989; Pogue et al., 1992b). Our thermal model suggests that this unconformity may be related to a significant cooling phase during Late Devonian to Permian time (Figures 3 and 4). This cooling event was likely associated with a period of exhumation and erosion that coincided with the postulated timing of Late Palaeozoic rifting and Carboniferous-Permian regional glacial erosion, which are documented in the stratigraphic successions of both the Peshawar Basin in Pakistan and the Kashmir and Zanskar area in India (Garzanti et al., 1996; Pogue et al., 1992a). Published seismic data and stratigraphic relationships in the SR suggest the presence of vertical normal faults in the Indian crystalline basement (Baker et al., 1988; Qayyum et al., 2015). In the Eastern and Central SR, Permian strata lie on top of Cambrian strata, forming a gently dipping (<2°) angular unconformity (Figure 2); however, in the Western SR, Cambrian strata are not preserved and Permian strata lie directly on top of the Neoproterozoic Salt Range Formation (Figure 5). We propose that normal faulting observed in published seismic data formed half graben structures that, in combination with regional erosion, could explain the Late Palaeozoic cooling recorded by our samples and formation of the unconformity in the SR (Figure 5).

5.2 | Pliocene development of the SRT

Himalayan foreland sedimentation (~18–5 Ma) buried the Precambrian-Eocene strata beneath 2–5 km of sediments in the SR (Johnson et al., 1985; Najman et al., 2003). Thermal models of the Khewra, Karoli and Pail transects show that final cooling was underway by 4–7 Ma (Figure 4c), while thermal models of the Western SR, located above a lateral ramp of the SRT, show that cooling started at 4–9 Ma (Figure 3). We favour our model results for the thrust front (Figure 4a), which combine 10 Cambrian to Permian samples from the three transects, indicating that most of the cooling associated with the SRT occurred after ~4 Ma. The most likely reasons why some AHe grains have ≥10 Ma cooling ages are either because not all grains are completely reset due to variable inherited radiation damage or because there was also a small cooling event at 10 Ma (Grelaud et al., 2002; Qayyum et al., 2015).

The joint thermal model M3 (Figure 4a), when interpreted along with the structural cross-section (Figure 6) shows that significant cooling of the Cambrian–Permian samples occurred between ~4 and ~3 Ma, when samples were exhumed above the SRT ramp due to removal of foreland strata. Since ~3 Ma, the samples have remained essentially above the AHePRZ, consistent with samples translating along the hanging wall flat of the SRT. The Miocene AHe samples (KmKr, KmPa), located 15–20 km north of the thrust front, are interpreted to have cooled through the AHePRZ due to rock uplift above the SRT ramp since ~2 Ma. We suggest that clastic foreland strata were mostly eroded as the thrust sheet was translated across the SRT ramp,

13653121, 2021, 3, Downloaded from https://onlinelibrary.wiley.com/doi/10.1111/ter.12515 by Universitaetsbibliothek, Wiley Online Library on [22/09/2023]. See the Terms and Conditions (https://onlinelibrary.wiley.com/terms-and-conditions) on Wiley Online Library for rules of use; OA articles are governed by the applicable Creative Commons License

TABLE 4 Thermal model parameters of samples from the Salt Range, Pakistan

Model Transect & Modelling approach	Samples	Modelling approach	AHe ages	AFT ages	Time–Temperature box	Low-Temperature constraints	Modern temperature constraints	Iterations Burn-in–Post-burn-in
Khewra Transect (Figure 3)	KhKg	M1	4	1	1,000 – 0 Ma 75 ± 75°C	550–500 Ma, 15 ± 15°C 300–270 Ma, 15 ± 15°C 60–55 Ma, 15 ± 15°C 18–15 Ma, 15 ± 15°C	15 ± 15°C	1.5×10^5 –2.5×10^5
Karoli Transect (Figure 3)	KhKr, KuKr, TgKr, DaKr,WrKr	M2	16	4	1,000 – 0 Ma 75 ± 75°C	550–500 Ma, 15 ± 15°C 300–270 Ma, 15 ± 15°C 60–55 Ma, 15 ± 15°C 18–15 Ma, 15 ± 15°C	15 ± 15°C	1.5×10^5 –2.5×10^5
	KmKr	M1	3	--	30 – 0 Ma 75 ± 75°C	18–15 Ma, 15 ± 15°C	15 ± 15°C	1×10^5 –1×10^5
Pail Transect (Figure 3)	KuPa, BgPa,DaPa,WrPa	M2	7	4	1,000 – 0 Ma 75 ± 75°C	550–500 Ma, 15 ± 15°C 300–270 Ma, 15 ± 15°C 60–55 Ma, 15 ± 15°C 18–15 Ma, 15 ± 15°C	15 ± 15°C	1.5×10^5 –2.5×10^5
	KmPa	M1	3	1	30 – 0 Ma 75 ± 75°C	18–15 Ma, 15 ± 15°C	15 ± 15°C	1×10^5 –1×10^5
Western Salt Range Transect (Figure 3)	TbDk	M1	2	1	500 – 0 Ma 100 ± 100°C	300–270 Ma, 15 ± 15°C	15 ± 15°C	1×10^5–1×10^5
	WrZa	M1	3	1	500 – 0 Ma 75 ± 75°C	300–270 Ma, 15 ± 15°C	15 ± 15°C	1×10^5 –1×10^5
	WrNm	M1	3	1	500 – 0 Ma 75 ± 75°C	300–270 Ma, 15 ± 15°C	15 ± 15°C	1.5×10^5 –2.5×10^5
	TbSw,WrSw	M2	8	2	500 – 0 Ma 75 ± 75°C	300–270 Ma, 15 ± 15°C	15 ± 15°C	1×10^5 –1×10^5
Combined model Salt Range (Figure 4)	KhKg, KhKr, KuKr, TgKr, DaKr,WrKr, KuPa, BgPa,DaPa,WrPa	M3	27	8	1,000 – 0 Ma 75 ± 75°C	550–500 Ma, 15 ± 15°C 300–270 Ma, 15 ± 15°C 60–55 Ma, 15 ± 15°C 18–15 Ma, 15 ± 15°C	15 ± 15°C	1.5×10^5 –2.5×10^5

13653121, 2021, 3, Downloaded from https://onlinelibrary.wiley.com/doi/10.1111/ter.12515 by Universitaetsbibliothek, Wiley Online Library on [22/09/2023]. See the Terms and Conditions (https://onlinelibrary.wiley.com/terms-and-conditions) on Wiley Online Library for rules of use; OA articles are governed by the applicable Creative Commons License

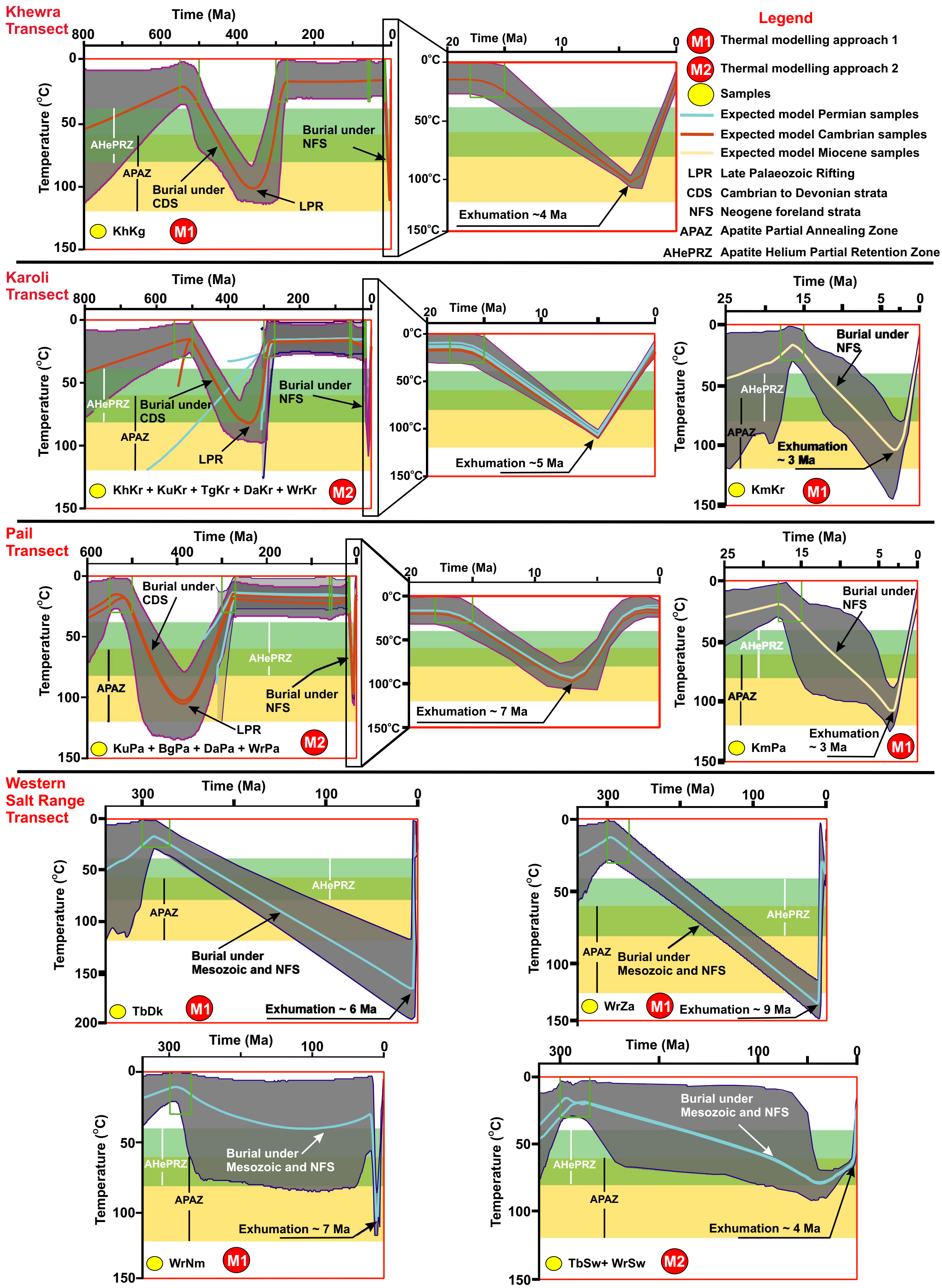

13653121, 2021, 3, Downloaded from https://onlinelibrary.wiley.com/doi/10.1111/ter.12515 by Universitaetsbibliothek, Wiley Online Library on [22/09/2023]. See the Terms and Conditions (https://onlinelibrary.wiley.com/terms-and-conditions) on Wiley Online Library for rules of use; OA articles are governed by the applicable Creative Commons License

FIGURE 3 Thermal history modelling results for the Khewra, Karoli, Pail and Western Salt Range transects. Thermal modelling of individual samples (M1) and multiple samples from the same transect (M2) are shown separately. Grey shaded areas represent elevated path probability and thick lines represent average model path (expected model) for the samples. The green boxes show depositional constraints. AHePRZ = Apatite helium partial retention zone, APAZ = Apatite partial annealing zone. Further details about modelling results are provided in the supplementary material section 3 [Colour figure can be viewed at wileyonlinelibrary.com]

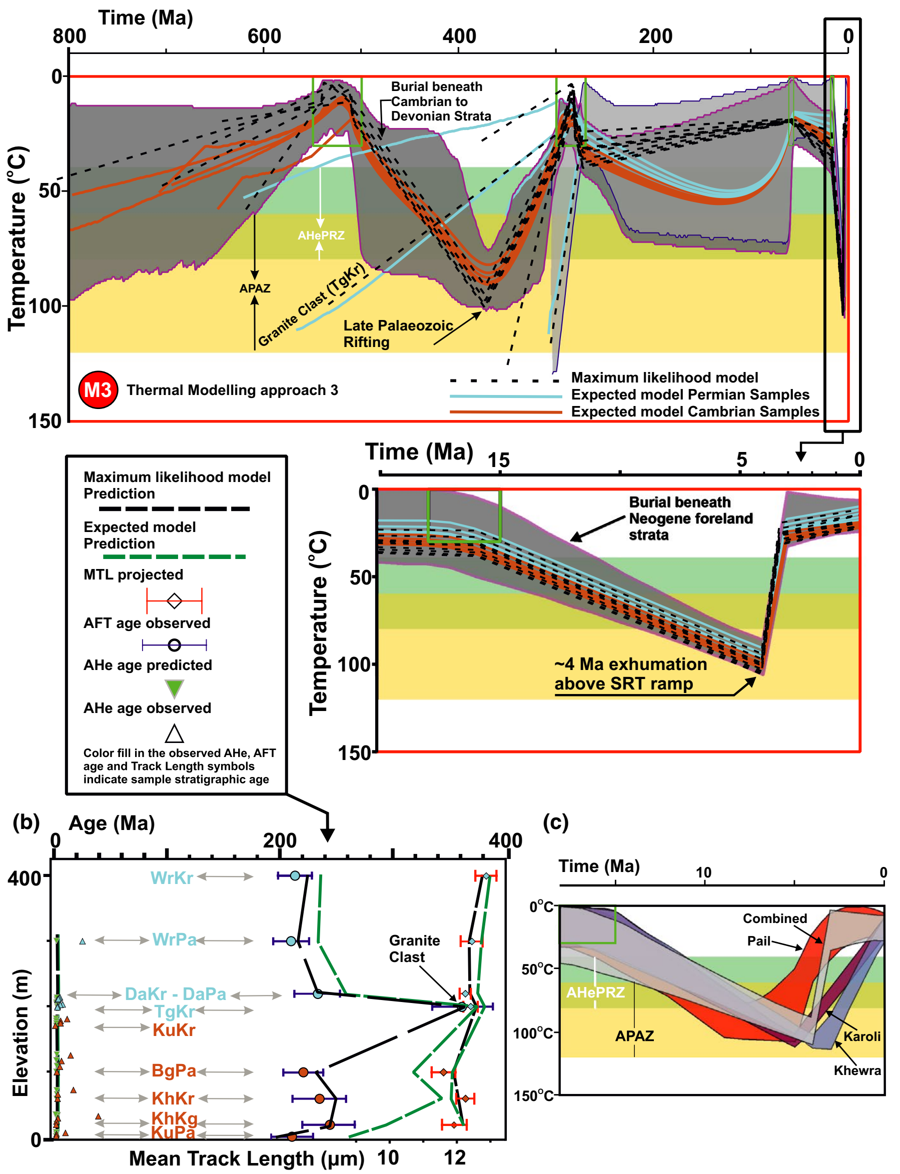

FIGURE 4 Thermal history modelling results performed using modelling approach M3. Cambrian and Permian samples from the Khewra, Karoli and Pail transects were combined in a single pseudo-vertical transect for thermal modelling. (a) Grey shaded area represents elevated path probability and thick lines represent average model path (expected model) for five Cambrian (brown lines) and five Permian samples (blue lines). Thick dashed lines represent best fit paths (maximum likelihood model) to the observed data for the Cambrian and Permian samples. The green boxes show depositional constraints. Red box extract shows thermal model for the last 20 myr. (b) Plot summarizing observed versus model (expected and maximum likelihood) predicted AHe, AFT ages and track lengths. (c) Comparison of Khewra, Karoli, Pail and combined thermal models for the last 18 Ma shows the range of the onset of exhumation. Further details about modelling results are provided in the supplementary material section 3. AHePRZ = Apatite helium partial retention zone, APAZ = Apatite partial annealing zone [Colour figure can be viewed at wileyonlinelibrary.com]

exposing Eocene carbonate rocks at the surface (Figure 6b). Since the Pliocene, the Pakistan Subhimalaya apparently had a semiarid climate (e.g. Dennell et al., 2006). In such conditions, the Eocene carbonate would be expected to experience limited erosion, thereby providing a resistant cap-rock protecting the underlying Cambrian–Palaeocene strata. The continued thrust sheet translation along the SRT hanging wall flat and exhumation of Cambrian–Eocene strata above the SRT ramp (Figure 6) is consistent with fault bend fold exhumation models (Baker et al., 1988; Burbank & Beck, 1989; Lock & Willett, 2008).

Based on our thermal model (Figure 4), we calculate a maximum exhumation rate of ~2.4–3.2 mm/yr between 3 and 4 Ma and almost negligible exhumation of our samples since 3 Ma. A minimum exhumation rate of ~0.6–0.8 mm/yr is calculated for the entire time span from 4 Ma to present. These calculations are based on the time when the Cambrian–Permian samples cooled below ~80–100°C, using a 25°C/km geothermal gradient and 20°C surface temperature. Combining the minimum shortening of 22 ± 2 km based on the restored schematic cross-section (Figure 6) and our ~ 4 Ma preferred onset for the SRT yields a minimum average shortening rate of 5–6 mm/yr, similar to the present-day shortening rate of ~5 mm/yr for the SRT in the Central SR (Jouanne et al., 2014). The timing and shortening rates of the SRT coincide with the 4–6 mm/yr shortening rate for frontal folds present on the eastern side of the Kashmir syntaxis (Gavillot et al., 2016, 2018).

13653121, 2021, 3, Downloaded from https://onlinelibrary.wiley.com/doi/10.1111/ter.12515 by Universitaetsbibliothek, Wiley Online Library on [22/09/2023]. See the Terms and Conditions (https://onlinelibrary.wiley.com/terms-and-conditions) on Wiley Online Library for rules of use; OA articles are governed by the applicable Creative Commons License

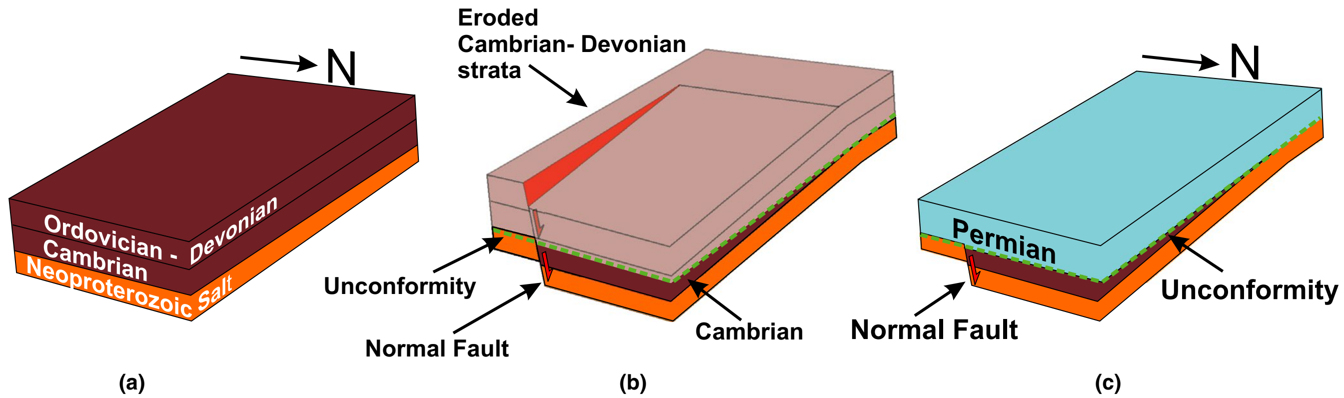

FIGURE 5 Schematic block diagram showing the Palaeozoic history of the Salt Range. (a) Cambrian–Devonian stratigraphy of the Salt Range. (b) Late Palaeozoic rifting and erosion of the Cambrian–Devonian strata. (c) Deposition of Permian strata unconformably above Cambrian and Neoproterozoic strata [Colour figure can be viewed at wileyonlinelibrary.com]

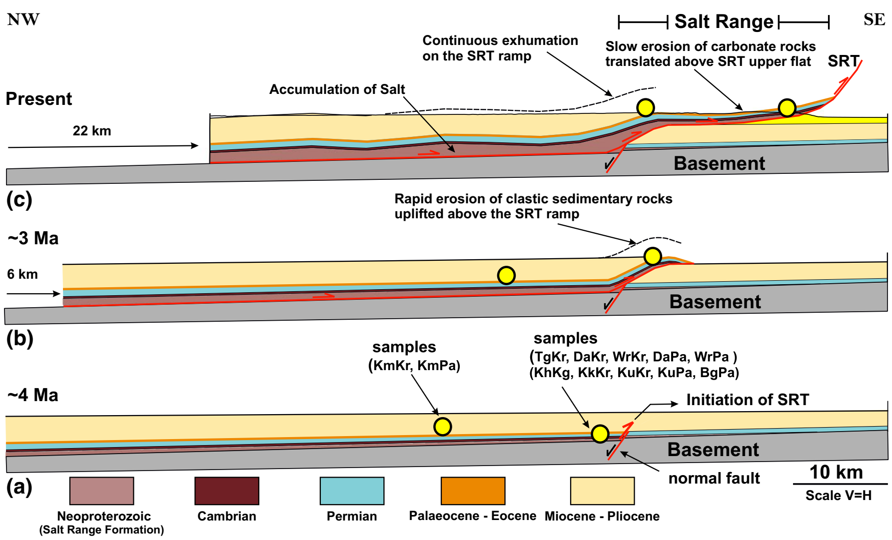

FIGURE 6 (a–c). Temporal development and exhumation pattern related to the SRT during the past 4 myr. (a) Undeformed cross-section showing the pre-existing normal fault in the basement. (b) Neogene foreland strata are removed from the thrust sheet as it passes over the SRT ramp between 4 and 3 Ma. (c) Translation of the SR thrust sheet towards the south above the SRT, forming a fault bend fold. The structural evolution model is based on MOVE modelling by Ghani et al. (2018) and previous studies by Baker et al. (1988). Horizontal and vertical scales are equal in the cross sections [Colour figure can be viewed at wileyonlinelibrary.com]

6 | CONCLUSIONS

The spatial distribution of cooling ages is controlled by their burial beneath foreland strata prior to exhumation. Thermal modelling of Cambrian–Permian samples shows that the present-day SR was affected by deformation associated with Late Palaeozoic rifting and regional erosion that resulted in the formation of a major unconformity. The SRT has been active since at least ~4 Ma with exhumation mainly focused above the SRT ramp. The comparable exhumation and shortening rates calculated for the SRT and the frontal fold structures of the Kashmir Himalaya highlight the contemporaneous evolution of structures on both sides of the Kashmir syntaxis.

ACKNOWLEDGEMENTS

We thank reviewers Yann Gavillot, Syed Ali Turab, Delores Robinson and associate editor Meinert Rahn for their detailed, critical reviews, corrections and suggestions for improving the article. Jean Braun is acknowledged for handling the manuscript. We thank the German Academic Exchange Service (DAAD) and the DFG (StRATEGy program) for financial assistance. We thank K. Gallagher and Petex for providing the QTQt and the MOVE programs for academic use.

ORCID

Humaad Ghani https://orcid.org/0000-0002-8878-8001

REFERENCES

Baker, D. M., Lillie, R. J., Yeats, R. S., Johnson, G. D., Yousuf, M., & Hamid, A. S. (1988). Development of the Himalayan frontal thrust zone: Salt Range, Pakistan. *Geology*, *16*, 3–7.

Brozovic, N., & Burbank, D. W. (2000). Dynamic fluvial systems and gravel progradation in the Himalayan foreland. *Geological Society of America Bulletin*, *112*(3), 394–412.

Burbank, D., & Beck, R. (1989). Early Pliocene uplift of the Salt Range; temporal constraints on the thrust wedge development, Northwest Himalaya, Pakistan. In L. L. Malinconico & R. J. Lillie (Eds.), *Tectonics of the Western Himalayas. Special Papers Geological Society of America*, *232*, 113–128.

Burbank, D. W., Beck, R. A., & Mulder, T. (1996). The Himalayan foreland basin. In A. Yin & T. M. Harrison (Eds.), *The tectonic evolution of Asia* (pp. 149–188). Cambridge University Press.

13653121, 2021, 3, Downloaded from https://onlinelibrary.wiley.com/doi/10.1111/ter.12515 by Universitaetsbibliothek, Wiley Online Library on [22/09/2023]. See the Terms and Conditions (https://onlinelibrary.wiley.com/terms-and-conditions) on Wiley Online Library for rules of use; OA articles are governed by the applicable Creative Commons License

Dennell, R., Coard, R., & Turner, A. (2006). The biostratigraphy and magnetic polarity zonation of the Pabbi Hills, northern Pakistan: An Upper Siwalik (Pinjor Stage) Upper Pliocene-Lower Pleistocene fluvial sequence. *Palaeogeography, Palaeoclimatology, Palaeoecology*, *234*(2–4), 168–185.

Farley, K. A. (2000). Helium diffusion from apatite: General behavior as illustrated by Durango fluorapatite. *Journal of Geophysical Research: Solid Earth*, *105*(B2), 2903–2914.

Farley, K. A. (2002). (U-Th)/He dating: Techniques, calibrations, and applications. *Reviews in Mineralogy and Geochemistry*, *47*(1), 819–844.

Gallagher, K. (2012). Transdimensional inverse thermal history modeling for quantitative thermochronology. *Journal of Geophysical Research. Solid Earth*, *117*(B2), B02408. https://doi.org/10.1029/2011JB008825

Gallagher, K., Brown, R., & Johnson, C. (1998). Fission track analysis and its applications to geological problems. *Annual Review of Earth and Planetary Sciences*, *26*(1), 519–572.

Garzanti, E., Angiolini, L., and Sciunnach, D. (1996). The Mid-Carboniferous to Lowermost Permian succession of Spiti (Po Group and Ganmachidam Formation; Tethys Himalaya, Northern India): Gondwana glaciation and rifting of Neo-Tethys. *Geodinamica Acta (Paris)*, *9*(2), 78–100.

Gavillot, Y., Meigs, A. J., Sousa, F. J., Stockli, D., Yule, D., & Malik, M. (2018). Late Cenozoic foreland-to-hinterland low-temperature exhumation history of the Kashmir Himalaya. *Tectonics*, *37*, 3041–3068.

Gavillot, Y., Meigs, A. J., Yule, D., Heermance, R., Rittenour, T., Madugo, C., & Malik, M. (2016). Shortening rate and Holocene surface rupture on the Riasi fault system in the Kashmir Himalaya: Active thrusting within the Northwest Himalayan orogenic wedge. *Geological Society of America Bulletin*, *128*(7–8), 1070–1094.

Gee, E. R., & Gee, D. G. (1989). Overview of the geology and structure of the Salt Range, with observations on related areas of northern Pakistan. *Geological Society of America Special Paper*, *232*, 95–112.

Ghani, H., Zeilinger, G., Sobel, E. R., & Heidarzadeh, G. (2018). Structural variation within the Himalayan fold and thrust belt: A case study from the Kohat-Potwar fold thrust belt of Pakistan. *Journal of Structural Geology*, *116*, 34–46.

Grelaud, S., Sassi, W., de Lamotte, D. F., Jaswal, T., & Roure, F. (2002). Kinematics of eastern Salt Range and South Potwar basin (Pakistan): A new scenario. *Marine and Petroleum Geology*, *19*(9), 1127–1139.

Hughes, N. C., Myrow, P. M., Ghazi, S., McKenzie, N. R., Stockli, D. F., & DiPietro, J. A. (2019). Cambrian geology of the Salt Range of Pakistan: Linking the Himalayan margin to the Indian craton. *Geological Society of America Bulletin*, *131*(7–8), 1095–1114.

Johnson, N. M., Stix, J., Tauxe, L., Cerveney, P. F., & Tahirkheli, R. A. K. (1985). Paleomagnetic chronology, fluvial processes, and tectonic implications of Siwalik deposits near Chinji village, Pakistan. *Journal of Geology*, *93*, 27–40.

Jouanne, F., Awan, A., Pecher, A., Kausar, A., Mugnier, J. L., Khan, I., Khan, N. A., & Melle, J. V. (2014). Present-day deformation of northern Pakistan from Salt Ranges to Karakoram Ranges. *Journal of Geophysical Research. Solid Earth*, *119*(3), 2487–2503.

Kadri, I. B. (1995). *Petroleum geology of Pakistan*. Pakistan Petroleum Limited.

Khan, M. A., & Raza, H. A. (1986). The role of geothermal gradients in hydrocarbon exploration in Pakistan. *Journal of Petroleum Geology*, *9*(3), 245–258.

Lock, J., & Willett, S. (2008). Low-temperature thermochronometric ages in fold-and-thrust belts. *Tectonophysics*, *456*, 147–162.

Meigs, A. J., Burbank, D. W., & Beck, R. A. (1995). Middle-Late Miocene (>10 Ma) formation of the Main Boundary thrust in the western Himalaya. *Geology*, *23*, 423–426.

Najman, Y., Garzanti, E., Pringle, M., Bickle, M., Stix, J., & Khan, I. (2003). Early-Middle Miocene paleodrainage and tectonics in the Pakistan Himalaya. *Geological Society of America Bulletin*, *115*(10), 1265–1277.

Pogue, K. R., DiPietro, J. A., Khan, S. R., Hughes, S. S., Dilles, J. H., & Lawrence, R. D. (1992a). Late Paleozoic rifting in northern Pakistan. *Tectonics*, *11*, 871–883.

Pogue, K. R., Wardlaw, B. R., Harris, A. G., & Hussain, A. (1992b). Paleozoic and Mesozoic stratigraphy of the Peshawar basin, Pakistan: Correlations and implications. *Geological Society of America Bulletin*, *104*, 915–927.

Qayyum, M., Spratt, D. A., Dixon, J. M., & Lawrence, R. D. (2015). Displacement transfer from fault-bend to fault-propagation fold geometry: An example from the Himalayan thrust front. *Journal of Structural Geology*, *77*, 260–276.

Turab, S. A., Stüwe, K., Stuart, F. M., Chew, D. M., & Cogne, N. (2017). Tectonics drives rapid exhumation of the western Himalayan syntaxis: Evidence from low-temperature thermochronometry of the Neelum valley region. *Pakistan. Lithosphere*, *9*(6), 874–888.

Van der Beek, P., Robert, X., Mugnier, J. L., Bernet, M., Huyghe, P., & Labrin, E. (2006). Late Miocene – Recent exhumation of the central Himalaya and recycling in the foreland basin assessed by apatite fission-track thermochronology of Siwalik sediments. *Nepal. Basin Research*, *18*, 413–434. https://doi.org/10.1111/j.1365-2117.2006.00305.x

SUPPORTING INFORMATION

Additional supporting information may be found online in the Supporting Information section.

Data S1. Paleozoic and Pliocene tectonic evolution of the Salt Range constrained by low-temperature thermochronology.

How to cite this article: Ghani H, Sobel ER, Zeilinger G, Glodny J, Zapata S, Irum I. Palaeozoic and Pliocene tectonic evolution of the Salt Range constrained by low-temperature thermochronology. *Terra Nova*. 2021;33:293–305. https://doi.org/10.1111/ter.12515

13653121, 2021, 3, Downloaded from https://onlinelibrary.wiley.com/doi/10.1111/ter.12515 by Universitaetsbibliothek, Wiley Online Library on [22/09/2023]. See the Terms and Conditions (https://onlinelibrary.wiley.com/terms-and-conditions) on Wiley Online Library for rules of use; OA articles are governed by the applicable Creative Commons License